

Complex Temporal Patterns of Large Earthquakes: Devil's Staircases

Yuxuan Chen^{*1}, Mian Liu¹, and Gang Luo²

ABSTRACT

Periodic or quasiperiodic earthquake recurrence on individual faults, as predicted by the elastic rebound model, is not common in nature. Instead, most earthquake sequences are complex and variable, and often show clusters of events separated by long but irregular intervals of quiescence. Such temporal patterns are especially common for large earthquakes in complex fault zones or regional and global fault networks. Mathematically described as the *Devil's Staircase*, such temporal patterns are a fractal property of nonlinear complex systems, in which a change of any part (e.g., rupture of a fault or fault segment) could affect the behavior of the whole system. We found that the lengths of the quiescent intervals between clusters are inversely related to tectonic-loading rates, whereas earthquake clustering can be attributed to many factors, including earthquake-induced viscoelastic relaxation and fault interaction. Whereas the underlying causes of the characteristics of earthquake sequences are not fully known, we attempted to statistically characterize these sequences. We found that most earthquake sequences are burstier than the Poisson model commonly used in probabilistic seismic hazard analysis, implying a higher probability of repeating events soon after a large earthquake.

KEY POINTS

- We ask whether large earthquakes occur periodically, randomly, or burstily, and why.
- We conclude that most large earthquakes occur burstily due to fault interaction and viscoelastic relaxation.
- The results imply a higher probability of repeating events after a large earthquake than do Poisson models.

[Supplemental Material](#)

INTRODUCTION

The elastic rebound model, introduced in the aftermath of the 1906 San Francisco earthquake (Reid, 1910), predicts cyclic stress buildup and release (via earthquakes) on a fault plane due to the relative motion of crustal blocks. Plate tectonics theory established in the 1960s explains such relative crustal motion across plate boundary faults. The steady relative motion of tectonic plates and finite strength of fault planes imply periodic or quasiperiodic occurrence of large earthquakes (i.e., characteristic earthquakes) on these faults. The recurrence time of these earthquakes is an important parameter for hazard assessment and therefore a focus of earthquake studies (Molnar, 1979; Youngs and Coppersmith, 1985; Atwater *et al.*, 2003).

Periodic or quasiperiodic earthquakes, however, are uncommon in nature. The Parkfield section of the San Andreas fault in California is perhaps the best-known example

for quasiperiodic earthquakes. Between 1857 and 1966, six M_w 6.0 events occurred there with an ~ 22 -year recurrence interval (Bakun and Lindh, 1985), but the next event, which took place in 2004, was overdue, challenging the simple elastic rebound model (Bakun *et al.*, 2005; Jackson and Kagan, 2006). In most fault systems in varied tectonic settings, large earthquakes are clustered in time, with long and variable quiescent intervals (Salditch *et al.*, 2019). Paleoseismic study by Sieh *et al.* (1989) at Pallett Creek, on the San Andreas fault in California, found clusters of large earthquakes with interevent times in several decades, but the length of the dormant periods between earthquake clusters is two to three centuries. In the Great Basin of western United States, paleoseismic data show clusters of events separated by long quiescent periods on individual faults or fault segments (Wallace, 1987). At the Africa–Eurasia plate boundary off west Algeria, Ratzov *et al.* (2015) analyzed a long record of turbidites and found that three clusters of earthquakes with durations of ~ 300 – 600 yr separated by two long quiescent periods of ~ 1600 yr. A similar pattern is found along the Dead Sea transform fault based on a 60,000-year record of seismites (Agnon, 2014). In Australia, rich

1. Department of Geological Sciences, University of Missouri, Columbia, Missouri, U.S.A.; 2. School of Geodesy and Geomatics, Wuhan University, Wuhan, China

*Corresponding author: yc2c@mail.missouri.edu

Cite this article as Chen, Y., M. Liu, and G. Luo (2020). Complex Temporal Patterns of Large Earthquakes: Devil's Staircases, *Bull. Seismol. Soc. Am.* **XX**, 1–13, doi: [10.1785/0120190148](https://doi.org/10.1785/0120190148)

© Seismological Society of America

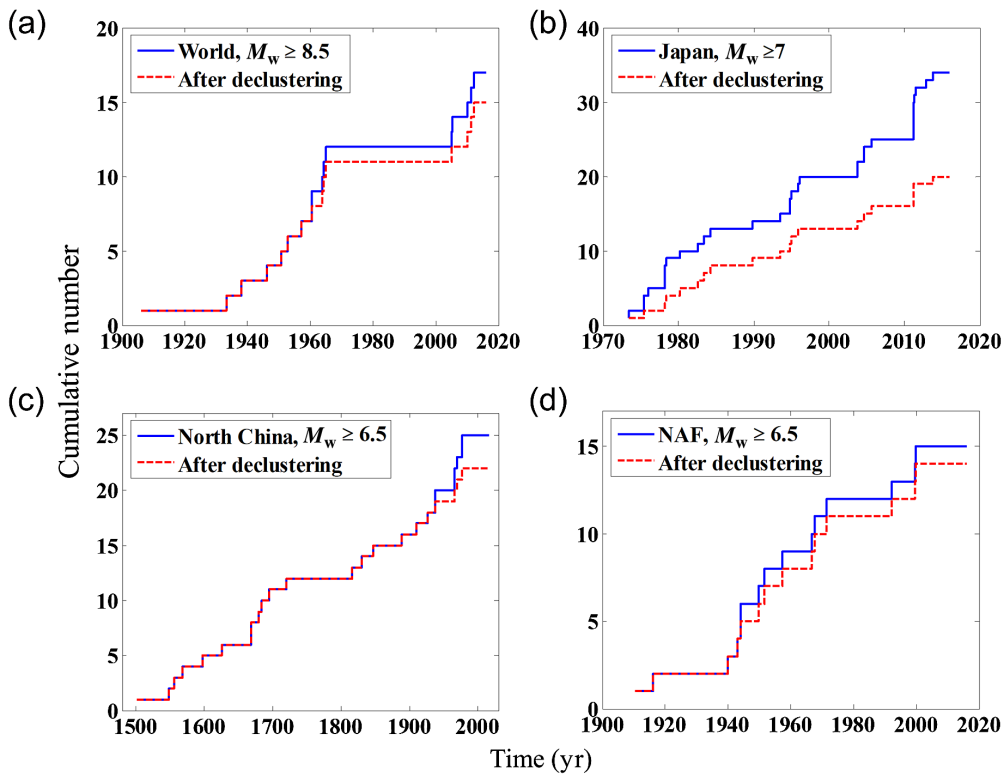


Figure 1. Temporal patterns of large earthquakes in (a) the world, (b) Japan, (c) North China, and (d) the North Anatolian fault (NAF). Solid lines are for the whole catalogs, and dashed lines are results after declustering, which has no clear effects on early records that have few large aftershocks. The color version of this figure is available only in the electronic edition.

morphogenic evidence of faulting across the continent commonly shows that a few large earthquakes within thousands of years are separated by much longer periods (10^4 – 10^6 yr) of quiescence on a single fault or proximal faults (Clark *et al.*, 2012, 2014).

In this study, we examine the temporal patterns of large shallow earthquakes. We show that, for fault systems of various scales, most earthquake sequences share common characteristics that can be described by the Devil’s Staircase, a fractal property of complex dynamic systems. We characterize these sequences statistically, explore the influencing tectonic factors, and discuss the implications for earthquake hazard assessment.

TEMPORAL PATTERNS OF LARGE EARTHQUAKES: DEVIL’S STAIRCASE

In this study, we focus on large shallow earthquakes ($M_w \geq 6$ and depth ≤ 60 km) because of the hazard that they pose and because they usually rupture multiple fault segments or faults, hence clearly deviating from simple elastic rebound models. We used the International Seismological Centre-Global Earthquake Model Global Instrumental Earthquake Catalogue (1904–2016) (Storchak *et al.*, 2013; Giacomo *et al.*, 2018). However, instrumentally recorded large earthquakes in

continental interiors and on individual faults or fault segments are often too few for vigorous statistical analysis. So, we also analyzed some sequences with historic and paleoseismic records. For North China, where historic earthquake record extends back to more than 2000 yr, we used a recently updated catalog (Cheng *et al.*, 2017).

Figure 1 shows the temporal patterns of large earthquakes in fault systems of different scales. Globally, $M_w \geq 8.5$ earthquakes show an irregular temporal pattern, with a long quiescent period (1965–2005) separating two active periods of clustered events (Fig. 1a). Similar patterns emerge for large events in tectonically active regions, such as Japan and California, with long periods of no or few events followed by clusters of several events within relatively short periods (Fig. 1b). In midcontinents, similar patterns are

found, but the quiescent intervals between earthquake clusters tend to be a few times longer than those in tectonically active regions (Fig. 1c). Such temporal patterns are found even on large individual faults (Fig. 1d).

Some of the earthquake clustering is likely due to dependent earthquakes (i.e., foreshocks and aftershocks). We used the method by Gardner and Knopoff (1974) to decluster catalogs. Earthquakes are grouped into different clusters according to time window T (days) and spatial window L (km) among them, which are defined as

$$\log_{10} T = \begin{cases} 0.032M + 2.7389, & \text{if } M \geq 6.5 \\ 0.5409M - 0.547, & \text{otherwise} \end{cases} \quad (1)$$

$$\log_{10} L = 0.1238M + 0.983, \quad (2)$$

in which M is the magnitude of a mainshock. For every cluster, the largest earthquake is identified as the mainshock, and other events within the space–time window are removed. We declustered the catalogs to see the impact of dependent earthquakes on the temporal patterns. Because large foreshocks or aftershocks are as important as mainshocks in terms of hazard,

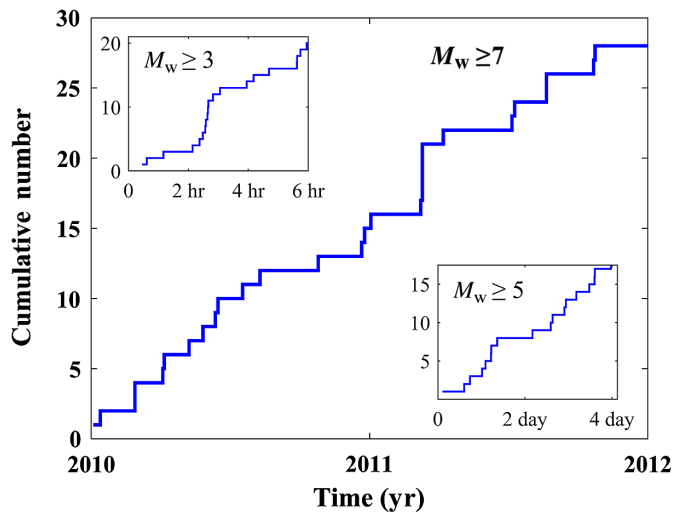


Figure 2. Temporal patterns of $M_w \geq 7$ earthquakes in the world. The insets show similar patterns for smaller events ($M_w \geq 5$ and $M_w \geq 3$, records start in 2010). The color version of this figure is available only in the electronic edition.

we use the whole catalogs for most of our statistical analysis in this study.

Figure 1 shows that declustering removes some events from the clusters, but the general patterns are unchanged: earthquakes are clustered within relatively short periods, which are separated by longer and variable intervals of quiescence. Such patterns are known mathematically as the “Devil’s Staircase” (Mandelbrot, 1982; Turcotte, 1997). The Devil’s Staircase is a fractal property of complex dynamic systems and can be constructed from the Cantor set. The Devil’s Staircase is commonly found in nature, including depositional sequences and the reversal of Earth’s magnetic field (Bak, 1996; Turcotte, 1997; De Michelis and Consolini, 2003; Simkin and Roychowdhury, 2014). A fractal property is scale invariant. In Figure 2, we show earthquake sequences with different lower cutoff magnitudes from the global catalog. They all show similar patterns of clusters of events separated by longer periods of inactivity.

CHARACTERIZING THE TEMPORAL PATTERNS

One way to characterize the temporal patterns of earthquakes is to fit the interevent times in earthquake catalogs with probability distribution functions (Fig. 3). Because all large earthquakes ($M_w \geq 6$) are potentially hazardous, we used the whole

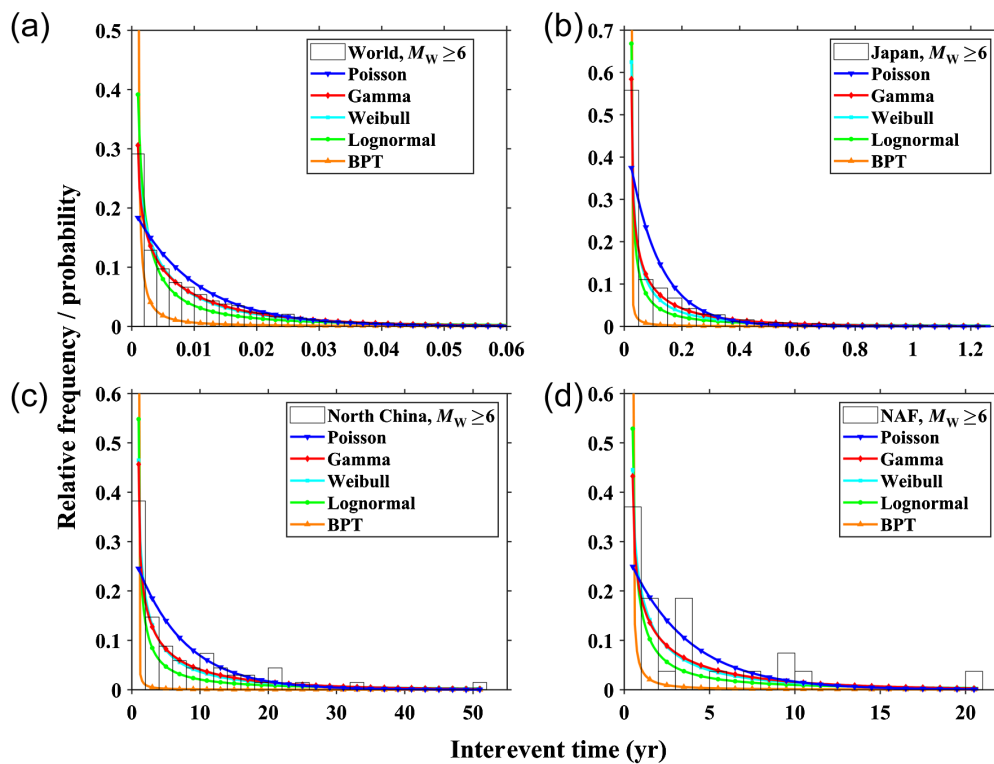


Figure 3. Comparison of the relative frequency (i.e., frequency scaled by the total number of events) histograms of the distribution of interevent times for different fault systems with probabilities (with same lengths of interevent time windows as the data) predicted by five probability models (curves). The closer a curve is to the centers of the tops of the histogram boxes, the better the curve fits the data. (a) World, (b) Japan, (c) North China, and (d) NAF. The color version of this figure is available only in the electronic edition.

catalogs for regions and faults that have a dozen or more events for statistical analysis (Table 1). We fit the interevent time data with probability models using the maximum-likelihood method. We tested five probability models (Poisson, gamma, Weibull, lognormal, and Brownian passage time [BPT]). All of them were used in previous studies on the interevent-time distribution of earthquakes (Table S1 and references, available in the supplemental material to this article).

The Poisson model assumes that, although the mean interval between events is known for a sequence, the exact time of each event to occur is random (the Poisson process). The interevent-time distribution of such a sequence follows an exponential distribution (Table S1). The Poisson model is simple (a one-parameter model) and commonly used

in probabilistic hazard analyses (Cornell, 1968; Working Group on California Earthquake Probabilities [WGCEP], 1988, 1995; Fujiwara *et al.*, 2006; Field *et al.*, 2009, 2014). It is a special case of the more generalized gamma and Weibull distributions (Table S1).

We investigated the distribution of interevent times of all the seismic sequences we studied. The relative frequency histograms show high frequency for events falling within short interevent times, and the frequency decreases rapidly with longer interevent times (Fig. 3). The pattern can be generally fit by all the five probability models (Fig. 3). We did Kolmogorov–Smirnov tests to statistically compare the fitting of these probability models with data (Tables S2–S5) and found that the gamma model fits the data best. Both the gamma and Weibull models fit better than the Poisson model, whereas the lognormal and BPT models fit worse, as can also be seen in Figure 3. Both the gamma and Weibull models have higher probability for short interevent times than the Poisson model. In other words, the data have tighter clusters, or are burstier, than the prediction of the Poisson model.

The variation of the interevent times can be measured by the coefficient of variation (COV), called the aperiodicity, which is defined by $\frac{\sigma_\tau}{\mu_\tau}$, the ratio of the standard deviation of interevent times (σ_τ) to the mean of interevent times (μ_τ) (Kagan and Jackson, 1991; Goes, 1996; Salditch *et al.*, 2019). For a sequence generated by a Poisson process, the COV value is 1. To measure the deviation from the Poisson model, we use a normalized COV, called the burstiness parameter (B) (Goh and Barabási, 2008), which is defined as

$$B = \frac{\frac{\sigma_\tau}{\mu_\tau} - 1}{\frac{\sigma_\tau}{\mu_\tau} + 1} = \frac{\sigma_\tau - \mu_\tau}{\sigma_\tau + \mu_\tau}. \quad (3)$$

The value of B ranges from -1 to 1 . $B = -1$ corresponds to a perfectly periodic sequence, because its $\sigma_\tau = 0$ (COV = 0). When $\sigma_\tau \gg \mu_\tau$, COV $\rightarrow \infty$ and $B \rightarrow 1$, which corresponds to

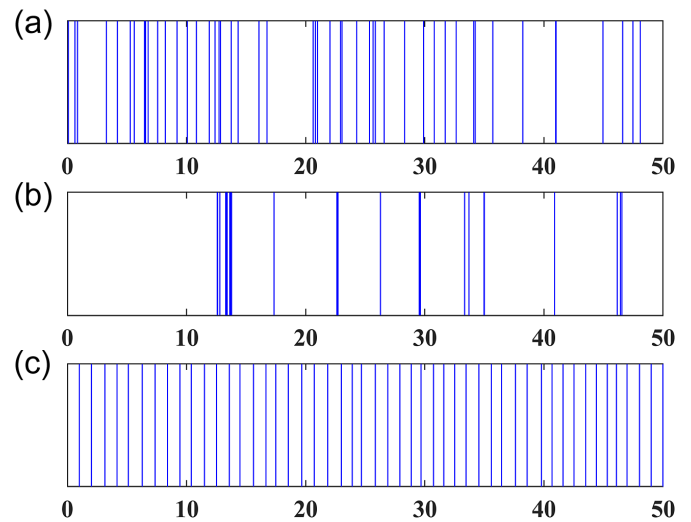


Figure 4. (a) A sequence of events generated by a Poisson model with $\mu = 1$. (b) A bursty sequence generated by the Weibull interevent-time distribution with $a = 0.3$, $b = 2$. (c) An antibursty sequence generated by the Gaussian interevent-time distribution with the mean $m = 1$ and the standard deviation $\sigma = 0.1$. The color version of this figure is available only in the electronic edition.

the most bursty sequence. $B = 0$ corresponds to a sequence produced by an ideal Poisson process with $\sigma_\tau = \mu_\tau$ (COV = 1) (Fig. 4a), for which the temporal activity pattern is random. Thus, a sequence is “bursty” when $0 < B < 1$ (Fig. 4b) and “quasiperiodic” when $-1 < B < 0$ (Fig. 4c).

The sequences with the same B -values can have a different order of events (Fig. 5). This difference can be described by the memory coefficient m , defined as the correlation coefficient of consecutive interevent time values over a sequence. That is, given all pairs of consecutive interevent times (τ_i, τ_{i+1}) (Goh and Barabási, 2008):

TABLE 1

Statistical Parameters of $M_w \geq 6$ Earthquakes in Different Tectonic Regions

Regions	Maximum Time Interval (yr)	Mean Time Interval (yr)	Burstiness Parameter	Memory Coefficient	Total Events	Removed Events	Time Period
World	0.12 (0.15)	0.010 (0.016)	0.10 (0.02)	0.07 (0.02)	5269	2054	1964–2016
Japan	1.27 (2.26)	0.11 (0.24)	0.23 (0.08)	0.25 (0.04)	840	465	1926–2016
Taiwan	3.29 (3.66)	0.73 (1.39)	0.05 (–0.11)	–0.11 (–0.36)	71	33	1964–2016
East African rift	14.57 (14.57)	1.66 (3.46)	0.31 (0.06)	0.00 (–0.02)	26	13	1964–2016
California	7.84 (7.84)	1.58 (2.11)	0.08 (–0.01)	0.35 (0.20)	53	13	1932–2016
New Zealand	6.40 (6.40)	1.21 (1.49)	0.09 (0.02)	–0.02 (–0.13)	61	11	1942–2016
Tibet	2.35 (2.35)	0.46 (0.66)	0.06 (–0.08)	0.21 (0.26)	111	33	1964–2016
Xinjiang	4.50 (4.50)	1.37 (1.95)	0.03 (–0.14)	–0.23 (–0.26)	38	11	1964–2016
North China	51.41 (51.41)	7.11 (8.63)	0.12 (0.04)	0.31 (0.25)	69	12	1500–2016

Results in the parentheses are obtained after declustering using the Gardner–Knopoff method (Gardner and Knopoff, 1974). The International Seismological Centre–Global Earthquake Model catalog for earthquake magnitudes larger than 6 is complete since 1964 (Michael, 2014). The local earthquake catalogs of Japan, California, and New Zealand start in 1926, 1934, and 1942, respectively, so are likely complete for $M_w \geq 6$ events. The North China catalog is complete for $M_w \geq 6$ events since 1291 (Huang *et al.*, 1994). We chose to use the catalog since 1500, to be conservative.

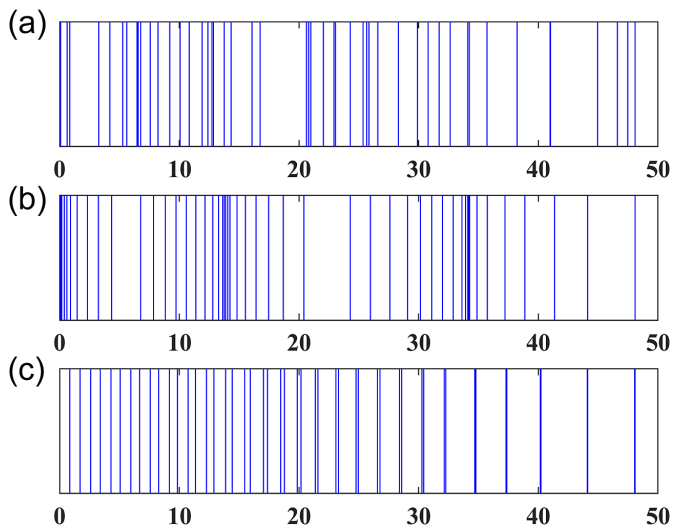


Figure 5. A bursty pattern can emerge through memory. The bursty pattern in (b) is obtained by shuffling the Poisson signals (a) to increase the memory effect (the short [long] interevent times tend to follow short [long] ones). A more regular pattern (c), with negative memory (short [long] interevent times tend to be followed by long [short] ones), is obtained by shuffling the sequence in (a). Note that sequences (a–c) have identical interevent-time distributions. The color version of this figure is available only in the electronic edition.

$$m = \frac{1}{n_\tau - 1} \sum_{i=1}^{n_\tau-1} \frac{(\tau_i - \mu_1)(\tau_{i+1} - \mu_2)}{\sigma_1 \sigma_2}, \quad (4)$$

in which n_τ is the number of interevent time measured from the sequence, μ_1 (μ_2) and σ_1 (σ_2) are the sample mean and sample standard deviation of the τ_i s (τ_{i+1} s) ($i = 1, \dots, n_\tau - 1$), respectively. The memory coefficient ranges from -1 to 1 . For sequences with $m > 0$, a short (long) interevent time tends to be followed by a short (long) one. A sequence with $m < 0$ tends to have a short (long) interevent time followed by a long (short) one.

We calculated the burstiness parameters and memory coefficients for earthquake sequences of faults ($M_w \geq 6.5$) and regions ($M_w \geq 6$) where available catalogs have more than a dozen events. The results are presented in Tables 1 and 2.

The burstiness parameters are close to but larger than 0 for all faults and regions studied before declustering (Tables 1 and 2), except that it is slightly negative for the Great Sumatran fault. Thus, the earthquake sequences are close to but burstier than ones produced by ideal Poisson processes. Removing dependent earthquakes decreases the values of burstiness parameters. The memory coefficients are complicated: they tend to be positive for regional sequences (Table 1) but negative for sequences for individual faults (Table 2).

We also calculated the burstiness parameters and memory coefficients for ruptures on five segments of the southern San Andreas compiled by Williams *et al.* (2019) from paleoseismic data (Table S6). For ruptures on each individual segment, the burstiness parameters are negative, or quasiperiodic as concluded by Williams *et al.* (2019). However, these segments are not isolated from each other. Some ruptures, including the 1857 Fort Tejon earthquake, ruptured multiple segments. When these segments are viewed as a whole, the burstiness parameter is slightly positive (i.e., bursty), similar to results for large individual faults based on instrumental and historical catalogs (Table 2). The memory coefficients are negative or close to zero, also similar to the results of other large individual faults (Table 2).

POSSIBLE TECTONIC FACTORS AND CAUSES

The Devil's Staircase pattern of large earthquakes is characterized by clusters of events separated by longer and irregular intervals of quiescence. Here, we examine how these features may be related to tectonic factors.

The length of quiescent intervals between earthquake clusters seems to be inversely related to tectonic loading rates (strain rates for tectonic regions or slip rates for individual faults; Fig. 6): lower loading rates correlate to longer quiescent intervals. The longest quiescent intervals also increase with the mean recurrence intervals, which is an indicator of average tectonic loading rate (Fig. 7). This is consistent with the very long intervals between earthquake clusters in Australia and other stable continents (Clark *et al.*, 2014), although we did not include those sequences in our analysis because of limited events in these sequences.

TABLE 2
Statistical Parameters of $M_w \geq 6.5$ Earthquakes on Individual Faults

Faults	Maximum Time Interval (yr)	Mean Time Interval (yr)	Burstiness Parameter	Memory Coefficient	Total Events	Removed Events	Time Period
Great Sumatran fault	18.69 (18.69)	6.23 (6.23)	-0.05 (-0.05)	-0.15 (-0.15)	16	0	1904–2016
North Anatolian fault	23.92 (23.92)	6.38 (6.88)	0.07 (0.04)	-0.06 (-0.13)	15	1	1904–2016
Sagaing fault	34.47 (34.47)	10.05 (12.56)	0.01 (-0.10)	0.23 (-0.03)	11	2	1904–2016
Xianshuihe fault	76.72 (76.72)	23.23 (23.23)	0.02 (0.02)	-0.34 (-0.34)	12	0	1700–2016

Results in the parentheses are obtained after declustering using the Gardner–Knopoff method (Gardner and Knopoff, 1974).

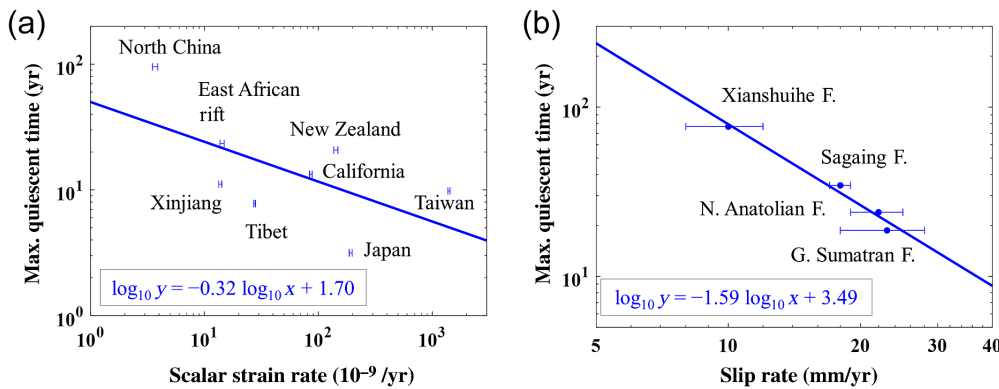


Figure 6. (a) The longest quiescent intervals for $M \geq 6.5$ earthquakes in various tectonic regions versus the magnitude of strain rates. The scalar strain rate data are from Kreemer *et al.* (2014). (b) The longest quiescent intervals for $M \geq 6.5$ earthquakes on individual faults versus the slip rates. Sources of slip rates: Genrich *et al.* (2000) for the Great Sumatran fault; Straub *et al.* (1997) and McClusky *et al.* (2000) for the NAF; Vigny *et al.* (2003) for the Sagaing fault; and Shen *et al.* (2005) for the Xianshuihe fault. Solid lines are least-square fitting. The insets show the regression formulas. The color version of this figure is available only in the electronic edition.

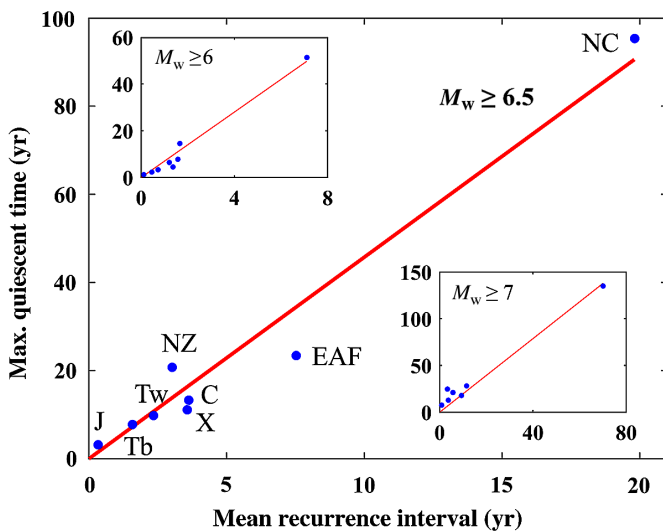


Figure 7. Relationship between mean recurrence interval and maximum quiescent time of $M_w \geq 6.5$ earthquakes in different tectonic regions (C, California; EAF, East African rift; J, Japan; NC, North China; NZ, New Zealand; Tb, Tibet; Tw, Taiwan; X, Xinjiang region, China). The insets show similar patterns for different cutoff magnitudes ($M_w \geq 6$ and $M_w \geq 7$). The color version of this figure is available only in the electronic edition.

For the active periods of clustered events, the tectonic control is more complex. The average number of events in each cluster seems to be larger in tectonically active regions with higher loading rates and shorter mean recurrence time (Fig. 8a,b). The average lengths of the seismically active periods, however, are not clearly correlated with tectonic loading rate (Fig. 8c,d).

The physical causes of temporal clustering of earthquakes may be multiple, including both earthquake-induced changes

of frictional property and stress transfer. Viscoelastic stress relaxation and fault interaction are two relatively well-known mechanisms of earthquake-induced stress transfer (Freed and Lin, 1998; Li *et al.*, 2009; Stein and Liu, 2009; Luo and Liu, 2012). To explore how these two mechanisms may contribute to the Devil's Staircase patterns of earthquakes, we developed a simple numerical model with one or multiple faults within a region (Fig. 9a), using a visco-elasto-plastic finite-element code we developed (Luo and Liu, 2010, 2012, 2018). Details of

the numerical scheme are presented in these references.

The model includes a 20-kilometer-thick, elastoplastic upper crust on top of an 80-kilometer-thick, viscoelastic lower crust and upper mantle (Fig. 9a). The elastic modulus is 8.75×10^{10} Pa for the upper crust and 1.1×10^{11} Pa for the lower crust and upper mantle; the Poisson's ratio is 0.25. The viscosity for the viscoelastic layer (purple color in Fig. 9a) is 1.0×10^{20} Pa · s. These are conventional values (Turcotte and Schubert, 1982). Using other reasonable values does not change the conclusions of this work. The fault zones are represented by special fault elements in a 2-kilometer-thick, elastoplastic vertical wall that simulates earthquakes by strain softening. The model domain is loaded by the imposed velocity on the sides of the model domain as shown in Figure 9a. The top surface is free, and the bottom of the model is fixed vertically but free to move horizontally.

The model simulates the stress and strain rate fields by solving the equation of force equilibrium:

$$\frac{\partial \sigma_{ij}}{\partial x_j} + f_i = 0, \quad (5)$$

in which σ_{ij} is stress tensor ($i, j = 1, 2, 3$) and f_i is gravitational body force. For each timestep, the model calculates the incremental strain, which may include viscous, elastic, and plastic components, using the finite-element method (Li *et al.*, 2009; Luo and Liu, 2018).

In this model, earthquakes are simulated by strain softening when rocks in the fault zone are loaded to their yield stress (e.g., Jaeger *et al.*, 2007; Luo and Liu, 2009, 2010). The strain softening of fault elements associated with coseismic slips is simulated with the Drucker-Prager yield criterion (e.g., Drucker and Prager, 1952; Khan and Huang, 1995):

$$F(\sigma, \kappa) = \sqrt{J_2} + \alpha I_1 - \beta, \quad (6)$$

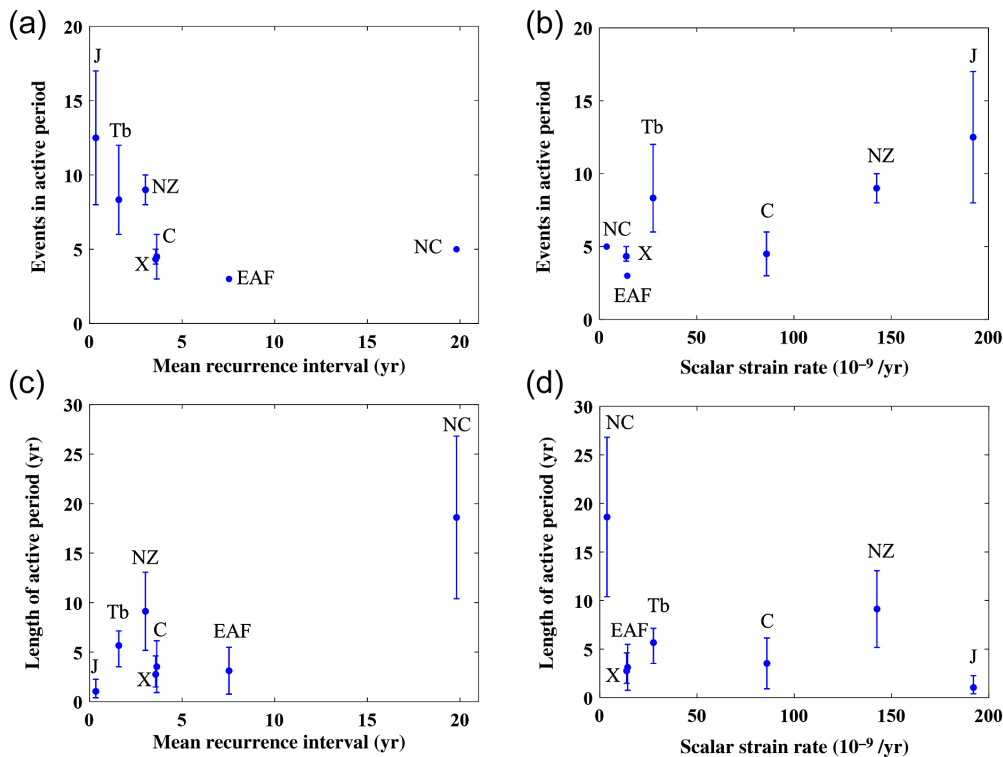


Figure 8. Relationship between features of earthquake clusters and tectonic factors for $M_w \geq 6.5$ earthquakes in different regions. (a,b) The number of events in active periods (clusters) versus mean recurrence intervals and regional strain rate, respectively. (c,d) The length of active periods versus mean recurrence intervals and regional strain rate, respectively. Abbreviations for tectonics regions are explained in Figure 7. The color version of this figure is available only in the electronic edition.

in which I_1 is the first invariant of the stress tensor; J_2 is the second invariant of the deviatoric stress tensor; and α and β are parameters of the Drucker–Prager yield criterion, related to cohesion and internal friction.

Our numerical experiments started from an initial stress field that equals the lithostatic stress (normal stresses equal to the weight of overlying materials and no shear stress). The density is 2800 kg/m^3 for the upper layer and 3200 kg/m^3 for the lower layer (Fig. 9a). We simulate synthetic seismicity after the model domain has been loaded to a quasi-steady state and the regional stress patterns have stabilized. We assume that an earthquake occurs when the stress reaches the Drucker–Prager yield criterion on a fault, and use a preset cohesion drop (5 MPa) to control the amount of strain softening. The internal friction angle and cohesion for the faults are 5° and 20 MPa, respectively (20° and 30 MPa for the rest of the upper crust). When an earthquake occurs on a fault, it is assumed that the whole fault plane fails uniformly.

When only one fault is included in the model and the entire model domain is assumed to be elastic, steady loading imposed on the sides of the model domain produces repeated failure of the fault with regular recurrence times (Fig. 9b), as would be predicted by the elastic rebound model. However, with three

arbitrarily oriented faults included in the model and the model domain includes both an elastoplastic (seismogenic) upper crust and a viscoelastic lower crust and upper mantle, the failure patterns show clusters of events separated by longer intervals of inactivity (Fig. 9d). In this case, stress on each fault is perturbed by failures of other faults and by viscous relaxation of the lower crust and upper mantle that transfers stress back to the upper crust (Freed and Lin, 2001; Li *et al.*, 2009). The resulting temporal patterns of earthquakes, either for the whole system (three faults) or on a single fault, have the features of the Devil’s Staircase (Fig. 9c). Thus, stress changes from viscous relaxation and fault interaction are likely important factors contributing to the clustering of earthquakes.

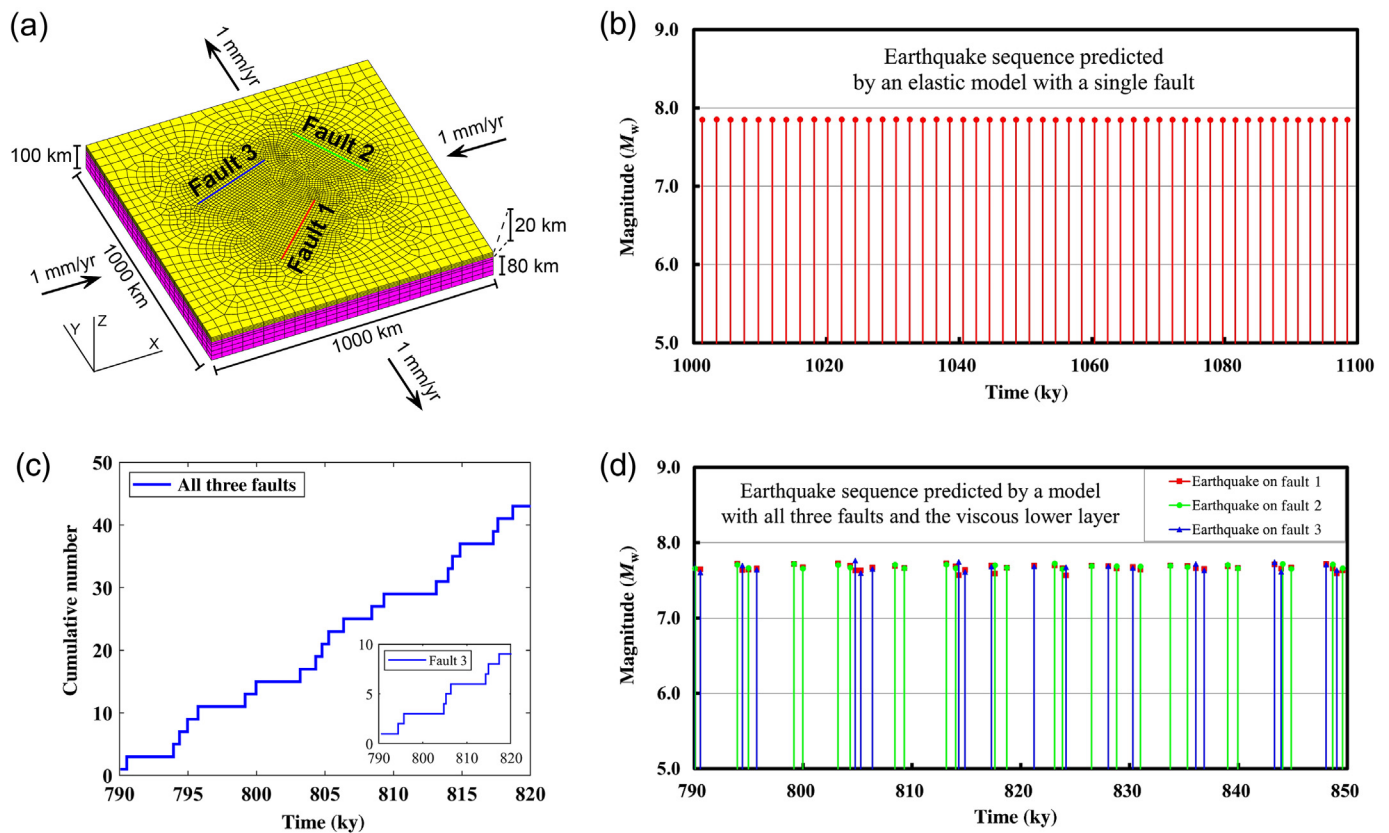
IMPLICATIONS FOR HAZARD ANALYSIS

The Devil’s Staircase patterns of large earthquakes have important implications for earthquake hazard assessment. First, the mean recurrence time, a key parameter for seismic hazard analysis, can vary drastically depending on which portion of the sequence the catalog represents. This can be a serious concern in hazard assessment, because catalogs for large earthquakes are often too short to reflect their complete temporal pattern, and it is difficult to know whether the few events in a catalog occurred within an earthquake cluster or spanned both clusters and quiescent intervals. For the same reason, we need to be cautious when assessing whether an event is “overdue” just because the time measured from the previous event has passed some “mean recurrence time” based on an incomplete catalog, as discussed by Salditch *et al.* (2019).

Second, probability seismic hazard analysis usually uses the conditional probability, which is defined by

$$P(T \leq \tau \leq T + \Delta T | \tau > T) = \frac{\int_T^{T+\Delta T} f(\tau) d\tau}{\int_T^\infty f(\tau) d\tau}, \quad (7)$$

in which τ is the interevent time, T is the time interval since the last earthquake in a catalog, ΔT is the prediction interval, and $f(\tau)$ is the probability density function of the interevent time. It



gives the probability of the next earthquake in the interval $(T, T + \Delta T)$ when knowing that no earthquake occurred before this interval since the last earthquake. For the Poisson model, which is commonly used in seismic hazard analysis (WGCEP, 1988, 1995, 2003; Field *et al.*, 2015), the conditional probability is a constant (see supplemental material to this article), so the Poisson model is also called the time-independent model. In other words, each event in the sequence is independent of other events. However, our results suggest that most earthquake sequences, especially when dependent events are not excluded, are burstier than a Poisson sequence and may be better fit by the gamma or Weibull distributions. The conditional probability of both the gamma and Weibull models is higher than that of the Poisson model for a small T but decreases as T increases (Fig. S2). In other words, the probability of repeating events soon after a large earthquake is higher than that predicted by the commonly used Poisson model. This is clear from the histograms of earthquakes sequences (Fig. 3). These repeating events could be aftershocks or events triggered by stress transferred from the preceding events. Recent examples are plenty, including the 1999 M_w 7.1 Hector Mine earthquake following the 1992 M_w 7.3 Lander earthquake in southern California (Freed and Lin, 2001), and the 2013 M_w 6.6 Lushan earthquake following the 2008 M_w 7.9 Wenchuan earthquake on the Longmenshan fault in the eastern Tibetan plateau (Liu *et al.*, 2014). Kagan and Jackson (1999) shows that doublets of large shallow earthquakes,

Figure 9. Numerical simulation of intraplate earthquakes. (a) Model setting and numerical mesh. The seismogenic upper crust is elastoplastic, sitting on top of a viscoelastic layer (lower crust and upper mantle). The model domain is loaded by the imposed velocity (vectors) on the sides. (b) Earthquake sequence predicted by a model that includes only one fault (fault 1) and without the viscoelastic lower layer. Time is since the beginning of the numerical experiment. (c) Temporal patterns of earthquakes for the fault system (all three faults). Inset is the pattern on fault 3. (d) Earthquake sequence predicted by a model with the three faults and both an elastoplastic upper layer and a viscoelastic lower layer. The color version of this figure is available only in the electronic edition.

with partly overlapped rupture zones and significantly shorter interevent time than the time needed for strain accumulation, are pervasive worldwide.

Finally, the Devil's Staircase patterns are characteristic of complex dynamic systems, which are nonlinear systems composed of many components (here, faults and fault segments) that interact with each other to produce nonlinear system behaviors. Small changes in some components can lead to big changes in the system. Short-term fault behavior in such a fault system is much more difficult to predict than faults experiencing cyclic loading and release. Nonetheless, one can try to forecast the system behavior of such fault systems. The best-fitting probability distribution function of a sequence can be inverted to generate pseudorandom interevent times that obey the same probability distribution (Devroye, 1986).

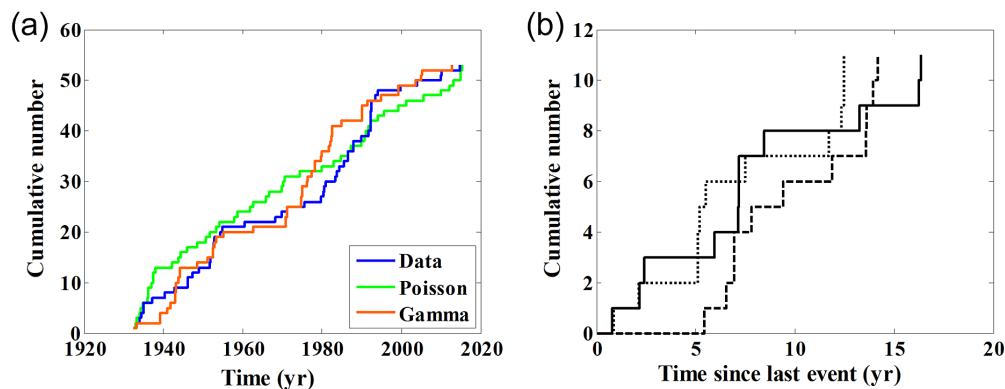


Figure 10. (a) Comparison of the temporal patterns of large ($M_w \geq 6$) earthquakes in California with those predicted by the best-fitting probability functions. (b) Three forecasted sequences for future $M_w \geq 6$ events in California after the last event in the catalog (24 August 2014), based on the best-fitting gamma probability distribution (Table S7). The color version of this figure is available only in the electronic edition.

For example, Figure 10a shows the instrumentally recorded $M_w \geq 6$ earthquakes in California and the sequences generated by the best-fitting Poisson and gamma probability distributions. The gamma model fits the general features of the data better than the Poisson model.

Inverting the best-fitting gamma distribution function, we can forecast the temporal feature of future $M_w \geq 6$ earthquake sequence in California (Fig. 10b). The forecast is nonunique; nonetheless, it indicates the statistical behavior of the regional fault system. Three forecasted sequences are shown here. They suggest that the future sequence of earthquakes will likely occur in clusters separated by relatively long and variable quiescent intervals, that is, Devil's Staircase.

DISCUSSION

In earthquake studies, much effort has been devoted to establishing the recurrence times of large earthquakes on a given fault to assess the probability of the next event occurring within a certain range of times (McCalpin and Nishenko, 1996; Biasi *et al.*, 2002, 2015). The elastic rebound model explains the basic physics of earthquake recurrence and predicts periodic or quasiperiodic earthquakes.

Establishing the temporal patterns of large earthquakes on individual faults, however, is difficult because large earthquakes are infrequent, and the catalogs are usually too short and incomplete. Quasiperiodic recurrence of large earthquakes has been reported on the Alpine fault, in the south-central Chile subduction zone, on the southern San Andreas fault, and on the intraplate Loma Blanca fault (Scharer *et al.*, 2010; Berryman *et al.*, 2012; Williams *et al.*, 2017; Moernaut *et al.*, 2018). In the first two cases, large earthquakes occurred on simple fault structures with a steadily high loading rate, so the elastic rebound model might work (Berryman *et al.*, 2012). In the last two cases, although the earthquake sequences appear to be quasiperiodic,

they also contain notable clusters (Weldon *et al.*, 2004; Williams *et al.*, 2017). When regional fault systems are considered, the earthquake sequences generally deviate from quasiperiodic patterns. Instead, they are bursty, with clusters of events separated by relatively long and irregular intervals of quiescence as Devil's Staircases.

The complexities of the temporal patterns of earthquakes may be partly attributed to data limitations. Instrumental catalogs may not be long enough to show statistically robust temporal patterns. For large earthquakes

in continental interiors where large earthquakes are less frequent than in plate boundary zones, historic and paleoseismic data may be needed, but they come with the associated uncertainties. Some of the earthquake clustering can certainly be attributed to aftershocks or foreshocks, and we have shown that declustering would reduce the burstiness in earthquake sequences. However, large aftershocks or foreshocks are as important as mainshocks when hazard is concerned and therefore should be included in hazard analysis.

On the other hand, there are good reasons not to expect large earthquakes to be quasiperiodic, because they violate the key premises of the elastic rebound model. First, the loading rate may not be constant, even for plate boundary faults (Friedrich *et al.*, 2003; Benedetti *et al.*, 2013; Ratzov *et al.*, 2015). Although the rates of relative plate motion have been steady during the past few million years (DeMets *et al.*, 1994), plate boundary faults are usually not a single fault plane but a system of fault branches and segments. The San Andreas fault, for example, consists of a complex system of subparallel faults in southern California that shares the loading from the relative Pacific–North American plate motion. Large earthquakes on one fault of this fault system could affect stress and loading rates on the other faults (Dolan *et al.*, 2007; Luo and Liu, 2012). For intraplate faults, the loading rates are lower and more variable than for plate boundary faults, because tectonic loading from plate boundaries is collectively accommodated by a widespread network of faults (Li *et al.*, 2009; Liu and Stein, 2016). On each individual fault, the loading rate is likely variable, affected by previous earthquakes on the fault, earthquakes on other faults in the system, and transient local stress perturbations such as erosion (Calais *et al.*, 2010).

Second, the elastic rebound model assumes cyclic strain accumulation and release on a given fault plane, but large earthquakes often rupture multiple and variable fault segments

(e.g., the 2001 M_w 7.8 Kunlun, China, earthquake) and faults (e.g., the 2016 M_w 7.8 Kaikōura, New Zealand, earthquake), making the concept of periodic release of strain energy on a defined fault plane inadequate. When seismicity in a regional network of faults is considered, the simple elastic rebound model does not apply.

The nonlinear and complex temporal patterns of large earthquakes have long been observed (Sieh *et al.*, 1989; Xu and Deng, 1996; Clark *et al.*, 2012). Some called these sequences supercycles (Salditch *et al.*, 2019). We have shown that the sequences of large earthquakes on fault systems of different scales show similar features of the Devil's Staircase, with clusters of events separated by long and variable intervals of quiescence. This suggests that large ruptures of faults behave like nonlinear complex dynamic systems, as noted in previous studies (Li *et al.*, 2009; Calais *et al.*, 2016; Liu and Stein, 2016).

This is not surprising, as fault systems in nature are known to be complex systems (Turcotte and Malamud, 2002). One evidence is the Gutenberg–Richter frequency–magnitude relationship, a power-law (fractal) distribution that is valid both regionally and globally (Turcotte, 1997). Complex systems are nonlinear dynamic systems composed of many components (here faults and fault segments) that interact with each other, producing nonlinear system behaviors. The clustering of earthquakes could arise from such interactions. Fault interaction includes transfer of static stress (the Coulomb stress) from a ruptured fault (or fault segment) to neighboring faults (or fault segments), as well as perturbation of regional loading conditions by local fault ruptures. It also includes stress transfer from the ductile lower crust to the upper crust by viscoelastic stress relaxation. Large earthquakes may also be triggered far from aftershock zones by dynamic stresses when seismic waves propagate. Fault interaction in a complex dynamic system is the key to understanding spatiotemporal variations of large earthquakes, especially those in continental interiors (Liu and Stein, 2016).

For a complex dynamic system of faults, the prediction or forecasting of fault ruptures is more difficult than expected from existing models based on elastic rebound. Nonetheless, we could try to characterize their temporal patterns to learn about the system behavior. We have shown that bursty sequences can be better fit by the gamma distribution function than the commonly used Poisson model. One implication is that soon after a large earthquake, the chance of having another one in the system is higher than that predicted by models assuming Poissonian occurrences of earthquakes, as suggested by numerous recent large earthquake sequences.

CONCLUSIONS

We found that the temporal patterns of large earthquakes, on individual faults or regional fault systems, show clusters of events separated by relatively long and variable intervals of seismic quiescence. Such patterns are characteristic of the

Devil's Staircase, a fractal property of nonlinear complex systems. For these earthquake sequences, the mean recurrence intervals, often estimated from records of the few most recent events, can vary significantly depending on whether these events are clustered in a relatively short active period or cover a spectrum of clusters and quiescent intervals.

The lengths of the quiescent intervals between clusters are inversely related to tectonic loading (or slip) rates. They are usually a few times longer than the periods of clustered events in tectonically active regions but can be thousands of years or longer in stable continental interiors. The earthquake clusters likely result from earthquake-induced stress transfer, including fault interaction and viscoelastic relaxation. The clustered events could include aftershocks and foreshocks. Because large aftershocks and foreshocks are as important as mainshocks in terms of seismic hazard, they should be included in seismic hazard analysis.

The burstiness of earthquake sequences can be statistically characterized using the burstiness parameter and the memory coefficient. The burstiness parameters for most earthquake sequences we studied have slightly positive values, meaning that these sequences are burstier than the Poisson process. The interevent times of most earthquake sequences can be better fitted by the gamma probability distribution than by the Poisson model. Models assuming a bursty gamma distribution (with positive burstiness parameter) predicts higher probabilities than models assuming a Poisson process for repeating events soon after a large earthquake, as indicated by numerous recent sequences of large earthquakes.

The Devil's Staircase distribution of large earthquakes implies that large fault ruptures, which often involve multiple segments or faults, behave as nonlinear complex systems. Prediction or forecasting of large earthquakes in such systems are much more difficult than for earthquakes on an isolated fault with simple structures under fast and steady tectonic loading. Thus, studying large earthquakes requires a system approach, rather than focusing only on stress accumulation and release on individual faults.

DATA AND RESOURCES

The catalogs of earthquakes in the World with small cutoff magnitudes ($M_w \geq 3$ and $M_w \geq 5$) used in Figure 2 were obtained from the International Seismological Centre, 2020, *On-line Bulletin* (doi: 10.31905/D808B830). In the supplemental material, we describe (1) probability distributions tested in this study, (2) best-fitting parameters for earthquake sequences in Figure 3, (3) best-fitting parameters for California earthquake sequences, and (4) conditional probabilities used in this study.

ACKNOWLEDGMENTS

The authors thank two anonymous reviewers for their detailed and constructive comments that improved the article. The authors thank Corné Kreemer for the strain rate data, and Jia Cheng for the M_w -

based earthquake catalog for China. The authors thank Seth Stein for helpful discussion. This work is supported by National Science Foundation (NSF) Grant 1519980. Luo acknowledges support from the project of the China Seismic Experimental Site (2019CSES0112) and the National Natural Science Foundation of China (41574085, 41974107).

REFERENCES

- Agnon, A. (2014). Pre-instrumental earthquakes along the Dead Sea rift, in *Dead Sea Transform Fault System: Reviews*, Springer, 207–261.
- Atwater, B. F., M. P. Tuttle, E. S. Schweig, C. M. Rubin, D. K. Yamaguchi, and E. Hemphill-Haley (2003). Earthquake recurrence inferred from paleoseismology, *Dev. Quaternary Sci.* **1**, 331–350.
- Bak, P. (1996). *How Nature Works: The Science of Self-Organized Criticality*, Springer Science & Business Media, New York, New York.
- Bakun, W. H., and A. G. Lindh (1985). The Parkfield, California, earthquake prediction experiment, *Science* **229**, 619–624.
- Bakun, W. H., B. Aagaard, B. Dost, W. Ellsworth, J. Hardebeck, R. Harris, C. Ji, M. Johnston, J. Langbein, and J. Lienkaemper (2005). Implications for prediction and hazard assessment from the 2004 Parkfield earthquake, *Nature* **437**, 969.
- Benedetti, L., I. Manighetti, Y. Gaudemer, R. Finkel, J. Malavieille, K. Pou, M. Arnold, G. Aumaitre, D. Bourles, and K. Keddadouche (2013). Earthquake synchrony and clustering on Fucino faults (Central Italy) as revealed from in situ ^{36}Cl exposure dating, *J. Geophys. Res.* **118**, 4948–4974.
- Berryman, K. R., U. A. Cochran, K. J. Clark, G. P. Biasi, R. M. Langridge, and P. Villamor (2012). Major earthquakes occur regularly on an isolated plate boundary fault, *Science* **336**, 1690–1693.
- Biasi, G. P., R. M. Langridge, K. R. Berryman, K. J. Clark, and U. A. Cochran (2015). Maximum-likelihood recurrence parameters and conditional probability of a ground-rupturing earthquake on the Southern Alpine Fault, South Island, New Zealand, *Bull. Seismol. Soc. Am.* **105**, 94–106.
- Biasi, G. P., R. J. Weldon, T. E. Fumal, and G. G. Seitz (2002). Paleoseismic event dating and the conditional probability of large earthquakes on the southern San Andreas fault, California, *Bull. Seismol. Soc. Am.* **92**, 2761–2781.
- Calais, E., T. Camelbeeck, S. Stein, M. Liu, and T. Craig (2016). A new paradigm for large earthquakes in stable continental plate interiors, *Geophys. Res. Lett.* **43**, doi: [10.1002/2016GL070815](https://doi.org/10.1002/2016GL070815).
- Calais, E., A. M. Freed, R. Van Arsdale, and S. Stein (2010). Triggering of New Madrid seismicity by late-Pleistocene erosion, *Nature* **466**, 608–611.
- Cheng, J., Y. Rong, H. Magistrale, G. Chen, and X. Xu (2017). An M_w -based historical earthquake catalog for Mainland China, *Bull. Seismol. Soc. Am.* **107**, 2490–2500.
- Clark, D., A. McPherson, and T. Allen (2014). Intraplate earthquakes in Australia, in *Intraplate Earthquakes*, Cambridge University Press, New York, New York, 49 pp.
- Clark, D., A. McPherson, and R. Van Dissen (2012). Long-term behaviour of Australian stable continental region (SCR) faults, *Tectonophysics* **566**, 1–30.
- Cornell, C. A. (1968). Engineering seismic risk analysis, *Bull. Seismol. Soc. Am.* **58**, 1583–1606.
- DeMets, C., R. G. Gordon, D. F. Argus, and S. Stein (1994). Effect of recent revisions to the geomagnetic reversal time scale on estimates of current plate motion, *Geophys. Res. Lett.* **21**, 2191–2194.
- De Michelis, P., and G. Consolini (2003). Some new approaches to the study of the Earth's magnetic field reversals, *Ann. Geophys.* **46**, 661–670.
- Devroye, L. (1986). Sample-based non-uniform random variate generation, *Proc. of the 18th Conf. on Winter Simulation*, ACM, 260–265.
- Dolan, J., D. Bowman, and C. Sammis (2007). Long-range and long-term fault interactions in Southern California, *Geology* **35**, doi: [10.1130/G23789A.1](https://doi.org/10.1130/G23789A.1).
- Drucker, D. C., and W. Prager (1952). Soil mechanics and plastic analysis for limit design, *Q. Appl. Math.* **10**, 157–165.
- Field, E. H., R. J. Arrowsmith, G. P. Biasi, P. Bird, T. E. Dawson, K. R. Felzer, D. D. Jackson, K. M. Johnson, T. H. Jordan, and C. Madden (2014). Uniform California Earthquake Rupture Forecast, version 3 (UCERF3)—The time-independent model, *Bull. Seismol. Soc. Am.* **104**, 1122–1180.
- Field, E. H., G. P. Biasi, P. Bird, T. E. Dawson, K. R. Felzer, D. D. Jackson, K. M. Johnson, T. H. Jordan, C. Madden, and A. J. Michael (2015). Long-term time-dependent probabilities for the third Uniform California Earthquake Rupture Forecast (UCERF3), *Bull. Seismol. Soc. Am.* **105**, 511–543.
- Field, E. H., T. E. Dawson, K. R. Felzer, A. D. Frankel, V. Gupta, T. H. Jordan, T. Parsons, M. D. Petersen, R. S. Stein, and R. Weldon (2009). Uniform California Earthquake Rupture Forecast, version 2 (UCERF 2), *Bull. Seismol. Soc. Am.* **99**, 2053–2107.
- Freed, A. M., and J. Lin (1998). Time-dependent changes in failure stress following thrust earthquakes, *J. Geophys. Res.* **103**, 24,393–24,409.
- Freed, A. M., and J. Lin (2001). Delayed triggering of the 1999 Hector Mine earthquake by viscoelastic stress transfer, *Nature* **411**, 180–183.
- Friedrich, A. M., B. P. Wernicke, N. A. Niemi, R. A. Bennett, and J. L. Davis (2003). Comparison of geodetic and geologic data from the Wasatch region, Utah, and implications for the spectral character of Earth deformation at periods of 10 to 10 million years, *J. Geophys. Res.* **108**, doi: [10.1029/2001JB000682](https://doi.org/10.1029/2001JB000682).
- Fujiwara, H., S. Kawai, S. Aoi, N. Morikawa, S. Senna, K. Kobayashi, T. Ishii, T. Okumura, and Y. Hayakawa (2006). National seismic hazard maps of Japan, *Bull. Earthq. Res. Inst. Univ. Tokyo* **81**, 221–232.
- Gardner, J., and L. Knopoff (1974). Is the sequence of earthquakes in Southern California, with aftershocks removed, Poissonian? *Bull. Seismol. Soc. Am.* **64**, 1363–1367.
- Genrich, J., Y. Bock, R. McCaffrey, L. Prawirodirdjo, C. Stevens, S. Puntodewo, C. Subarya, and S. Wdowski (2000). Distribution of slip at the northern Sumatran fault system, *J. Geophys. Res.* **105**, 28,327–28,341.
- Giacomo, D. D., E. R. Engdahl, and D. A. Storchak (2018). The ISC-GEM Earthquake Catalogue (1904–2014): Status after the Extension Project, *Earth Syst. Sci. Data* **10**, 1877–1899.
- Goes, S. D. (1996). Irregular recurrence of large earthquakes: An analysis of historic and paleoseismic catalogs, *J. Geophys. Res.* **101**, 5739–5749.
- Goh, K.-I., and A.-L. Barabási (2008). Burstiness and memory in complex systems, *Europhys. Lett.* **81**, 48002.

- Huang, W.-Q., W.-X. Li, and X.-F. Cao (1994). Research on the completeness of earthquake data in the Chinese mainland (I)—North China, *Acta Seismol. Sin.* **7**, 351–359.
- Jackson, D., and Y. Kagan (2006). The 2004 Parkfield earthquake, the 1985 prediction, and characteristic earthquakes: Lessons for the future, *Bull. Seismol. Soc. Am.* **96**, S397–S409.
- Jaeger, J. C., N. G. W. Cook, and R. W. Zimmerman (2007). *Fundamentals of Rock Mechanics*, Blackwell Publishing, Oxford, United Kingdom.
- Kagan, Y. Y., and D. D. Jackson (1991). Long-term earthquake clustering, *Geophys. J. Int.* **104**, 117–133.
- Kagan, Y. Y., and D. D. Jackson (1999). Worldwide doublets of large shallow earthquakes, *Bull. Seismol. Soc. Am.* **89**, 1147–1155.
- Khan, A. S., and S. Huang (1995). *Continuum Theory of Plasticity*, John Wiley & Sons Inc, New York, New York.
- Kreemer, C., G. Blewitt, and E. C. Klein (2014). A geodetic plate motion and Global Strain Rate Model, *Geochem. Geophys. Geosys.* **15**, 3849–3889.
- Li, Q., M. Liu, and S. Stein (2009). Spatiotemporal complexity of continental intraplate seismicity: Insights from geodynamic modeling and implications for seismic hazard estimation, *Bull. Seismol. Soc. Am.* **99**, doi: [10.1785/0120080005](https://doi.org/10.1785/0120080005).
- Liu, M., and S. Stein (2016). Mid-continental earthquakes: Spatiotemporal occurrences, causes, and hazards, *Earth Sci. Rev.* **162**, 364–386.
- Liu, M., G. Luo, and H. Wang (2014). The 2013 Lushan earthquake in China tests hazard assessments, *Seismol. Res. Lett.* **85**, 40–43.
- Luo, G., and M. Liu (2009). How does trench coupling lead to mountain building in the Subandes? A viscoelastoplastic finite element model, *J. Geophys. Res.* **114**, 1–16, doi: [10.1029/2008JB005861](https://doi.org/10.1029/2008JB005861).
- Luo, G., and M. Liu (2010). Stress evolution and fault interactions before and after the 2008 Great Wenchuan earthquake, *Tectonophysics* **491**, 127–140, doi: [10.1016/j.tecto.2009.12.019](https://doi.org/10.1016/j.tecto.2009.12.019).
- Luo, G., and M. Liu (2012). Multi-timescale mechanical coupling between the San Jacinto fault and the San Andreas fault, southern California, *Lithosphere* **4**, doi: [10.1130/L180.1](https://doi.org/10.1130/L180.1).
- Luo, G., and M. Liu (2018). Stressing rates and seismicity on the major faults in eastern Tibetan Plateau, *J. Geophys. Res.* **123**, doi: [10.1029/2018JB015532](https://doi.org/10.1029/2018JB015532).
- Mandelbrot, B. B. (1982). *The Fractal Geometry of Nature*, W. H. Freeman, New York, New York.
- McCalpin, J., and S. Nishenko (1996). Holocene paleoseismicity, temporal clustering, and probabilities of future large ($M > 7$) earthquakes on the Wasatch fault zone, Utah, *J. Geophys. Res.* **101**, 6233–6253.
- McClusky, S., S. Balassanian, A. Barka, C. Demir, S. Ergintav, I. Georgiev, O. Gurkan, M. Hamburger, K. Hurst, and H. Kahle (2000). Global Positioning System constraints on plate kinematics and dynamics in the eastern Mediterranean and Caucasus, *J. Geophys. Res.* **105**, 5695–5719.
- Michael, A. J. (2014). How complete is the ISC-GEM global earthquake catalog? *Bull. Seismol. Soc. Am.* **104**, 1829–1837.
- Moernaut, J., M. Van Daele, K. Fontijn, K. Heirman, P. Kempf, M. Pino, G. Valdebenito, R. Urrutia, M. Strasser, and M. De Batist (2018). Larger earthquakes recur more periodically: New insights in the megathrust earthquake cycle from lacustrine turbidite records in south-central Chile, *Earth Planet. Sci. Lett.* **481**, 9–19.
- Molnar, P. (1979). Earthquake recurrence intervals and plate tectonics, *Bull. Seismol. Soc. Am.* **69**, 115–133.
- Ratzov, G., A. Cattaneo, N. Babonneau, J. Déverchère, K. Yelles, R. Bracene, and F. Courboux (2015). Holocene turbidites record earthquake supercycles at a slow-rate plate boundary, *Geology* **43**, 331–334.
- Reid, H. F. (1910). The California earthquake of April 18, 1906, *Report of the State Investigation Commission*, in *The Mechanics of the Earthquake*, Vol. 2, 206 pp.
- Salditch, L., S. Stein, J. Neely, B. D. Spencer, E. M. Brooks, A. Agnon, and M. Liu (2019). Earthquake supercycles and Long-Term Fault Memory, *Tectonophysics* **228/289**, doi: [10.1016/j.tecto.2019.228289](https://doi.org/10.1016/j.tecto.2019.228289).
- Scharer, K. M., G. P. Biasi, R. J. Weldon, and T. E. Fumal (2010). Quasi-periodic recurrence of large earthquakes on the southern San Andreas fault, *Geology* **38**, 555–558.
- Shen, Z. K., J. Lü, M. Wang, and R. Bürgmann (2005). Contemporary crustal deformation around the southeast borderland of the Tibetan Plateau, *J. Geophys. Res.* **110**, doi: [10.1029/2004JB003421](https://doi.org/10.1029/2004JB003421).
- Sieh, K. E., M. Stuiver, and D. Brillinger (1989). A more precise chronology of earthquakes produced by the San Andreas fault in southern California, *J. Geophys. Res.* **94**, 603–623.
- Simkin, M., and V. Roychowdhury (2014). Stochastic modeling of a serial killer, *J. Theor. Biol.* **355**, 111–116.
- Stein, S., and M. Liu (2009). Long aftershock sequences within continents and implications for earthquake hazard assessment, *Nature* **462**, 87–89.
- Storchak, D. A., D. Di Giacomo, I. Bondár, E. R. Engdahl, J. Harris, W. H. Lee, A. Villaseñor, and P. Bormann (2013). Public release of the ISC-GEM global instrumental earthquake catalogue (1900–2009), *Seismol. Res. Lett.* **84**, 810–815.
- Straub, C., H. G. Kahle, and C. Schindler (1997). GPS and geologic estimates of the tectonic activity in the Marmara Sea region, NW Anatolia, *J. Geophys. Res.* **102**, 27,587–27,601.
- Turcotte, D. L. (1997). *Fractals and Chaos in Geology and Geophysics*, Cambridge University Press, New York, New York.
- Turcotte, D. L., and B. D. Malamud (2002). 14. Earthquakes as a complex system, *Int. Geophys.* **81**, 209–227.
- Turcotte, D. L., and G. Schubert (1982). *Geodynamics: Applications of Continuum Physics to Geological Problems*, John Wiley & Sons, New York, New York.
- Vigny, C., A. Socquet, C. Rangin, N. Chamot-Rooke, M. Pubellier, M. N. Bouin, G. Bertrand, and M. Becker (2003). Present-day crustal deformation around Sagaing fault, Myanmar, *J. Geophys. Res.* **108**, doi: [10.1029/2002JB001999](https://doi.org/10.1029/2002JB001999).
- Wallace, R. E. (1987). Grouping and migration of surface faulting and variations in slip rates on faults in the Great Basin province, *Bull. Seismol. Soc. Am.* **77**, 868–876.
- Weldon, R., K. Scharer, T. Fumal, and G. Biasi (2004). Wrightwood and the earthquake cycle: What a long recurrence record tells us about how faults work, *GSA Today* **14**, 4–10.
- Williams, R. T., J. R. Davis, and L. B. Goodwin (2019). Do large earthquakes occur at regular intervals through time? A perspective from the geologic record, *Geophys. Res. Lett.* **46**, doi: [10.1029/2019GL083291](https://doi.org/10.1029/2019GL083291).
- Williams, R. T., L. B. Goodwin, W. D. Sharp, and P. S. Mozley (2017). Reading a 400,000-year record of earthquake frequency for an

intraplate fault, *Proc. Natl. Acad. Sci. Unit. States Am.* **114**, 4893–4898.

Working Group on California Earthquake Probabilities (WGCEP) (1988). Probabilities of large earthquakes occurring in California on the San Andreas fault, *U. S. Geol. Surv. Open-File Rept.* 88-398, 62 pp.

Working Group on California Earthquake Probabilities (WGCEP) (1995). Seismic hazards in southern California: Probable earthquakes, 1994 to 2024, *Bull. Seismol. Soc. Am.* **85**, 379–439.

Working Group on California Earthquake Probabilities (WGCEP) (2003). Earthquake probabilities in the San Francisco Bay

Region, 2002-2031, *U. S. Geol. Surv. Open-File Rept.* 03-214, 235 pp.

Xu, X., and Q. Deng (1996). Nonlinear characteristics of paleoseismicity in China, *J. Geophys. Res.* **101**, 6209–6231.

Youngs, R. R., and K. J. Coppersmith (1985). Implications of fault slip rates and earthquake recurrence models to probabilistic seismic hazard estimates, *Bull. Seismol. Soc. Am.* **75**, 939–964.

Manuscript received 8 June 2019

Published online 14 April 2020